Geol. Mag. **147** (5), 2010, pp. 777–788. © Cambridge University Press 2010
doi:10.1017/S0016756810000154

Diopsidites from a Neoproterozoic–Cambrian suture in southern India

M. SANTOSH*†, V. J. RAJESH‡, T. TSUNOGAE§ & S. ARAI‡

*Department of Natural Environmental Science, Faculty of Science, Kochi University, Akebono-cho 2-5-1, Kochi 780-8520, Japan
†Department of Earth and Atmospheric Sciences, Center for Environmental Sciences, Saint Louis University, St. Louis MO 63108, USA
‡Department of Earth Sciences, Faculty of Science, Kanazawa University, Kakuma-machi, Kanazawa 920-1192, Japan
§Graduate School of Life and Environmental Sciences (Earth Evolution Sciences), University of Tsukuba, Ibaraki 305-8572, Japan

(*Received* 29 September 2009; *accepted* 9 December 2009; First published online 4 March 2010)

Abstract – We report the occurrence and characteristics of diopsidite dykes and veins from the Palghat-Cauvery Suture Zone (PCSZ) marking the boundary between the Archaean Dharwar craton to the north and the Proterozoic Madurai Block to the south, which is considered as a trace of the Cambrian Gondwana suture zone in southern India. The diopsidites are composed predominantly of coarse crystals of diopside [Mg no. (100 Mg/(Mg+Fe^{tot})) up to 89] surrounded by retrograde calcic amphibole, plagioclase and phlogopite with accessory titanite and calcite. The major, trace and rare earth element characteristics of the diopside crystals suggest their formation in a subduction zone setting. We correlate the petrogenesis of the diopsidites with the tectonics associated with the subduction and closure of the Neoproterozoic Mozambique Ocean prior to the final collisional assembly of the Gondwana supercontinent in Cambrian.

Keywords: diopsidite, subduction, suture zone, southern India, Gondwana.

1. Introduction

Diopsidites are calcic pyroxene-rich rocks occurring as dykes and veins mostly associated with mantle rocks in subduction settings. A pure (almost end member) diopside composition of calcic pyroxene (100 Mg/(Mg+Fe^{tot}) > 95) was reported by Python *et al.* (2007*a*,*b*) from diopsidite dykes in the mantle section of the Oman ophiolite. These dykes comprise mainly of diopside with traces of forsterite, anorthite, titanite or andradite together with hydrous minerals such as antigorite and tremolite. A similar suite of rocks called rodingites also act as 'Ca traps' and are interpreted to be derived from basaltic rocks by Ca-metasomatism. They are characterized by grossular garnet and diopside (±chlorite), clinozoisite, epidote, prehnite, albeit the rodingites formed at relatively low temperatures (< 450 °C) from gabbroic or clinopyroxenite precursors (e.g. Frost, 1975; Rice, 1983; Bach & Klein, 2008, 2009).

Diopsidites and rodingites are considered to be products of extreme Ca-metasomatism associated with the hydrothermal alteration of gabbroic massifs and dykes at the contact with ultramafic rocks in the ocean lithospheric mantle (e.g. Bach & Klein, 2009). The temperature at which diopsidites are formed is a subject of debate. Python *et al.* (2007*b*) interpreted these dykes as the product of high-temperature (~ 800 °C) hydrothermal circulation in the upper mantle section of the Oman ophiolite. However, based on thermodynamic modelling, Bach & Klein (2009) argued that diopsidites could also form at much lower temperatures and a study of the phase relations of diopsidites suggests that if garnet is also associated with diopside, then temperatures were probably below 450 °C.

The occurrence of diopside-rich dykes and veins has also been reported from accreted oceanic sections of various orogens. Pedrosa-Soares *et al.* (1998) described the association of diopsidite in association with metachert from the Salinas Formation located between the São Francisco and Congo cratons and correlated them with the remnants of a Neoproterozoic oceanic crust which was consumed through eastward subduction and formation of the Araçuaí–West Congo orogen. Quanru *et al.* (2006) reported diopsidites from the ophiolitic mélanges from the Eastern Himalayan syntaxis. Diopsidites also occur within the ophiolite mélange zone of Nurali in southern Urals (Gaggero *et al.* 1997). Coarse-grained diopsidites in association with dunites, peridotites and harzburgites were described within a subduction zone setting by Jan & Howie (1981) from the Jijal Complex of Kohistan in northwest Pakistan. Yang (2006) described clinopyroxene-rich rocks in associated with calcic garnet from the Hujialin region of the Su-Lu collisional belt in Eastern China and considered these rocks to represent the remnants of a deeply subducted arc cumulate.

In this report we present petrological and mineral chemical characteristics of diopsidites from

*Author for correspondence: santosh@cc.kochi-u.ac.jp

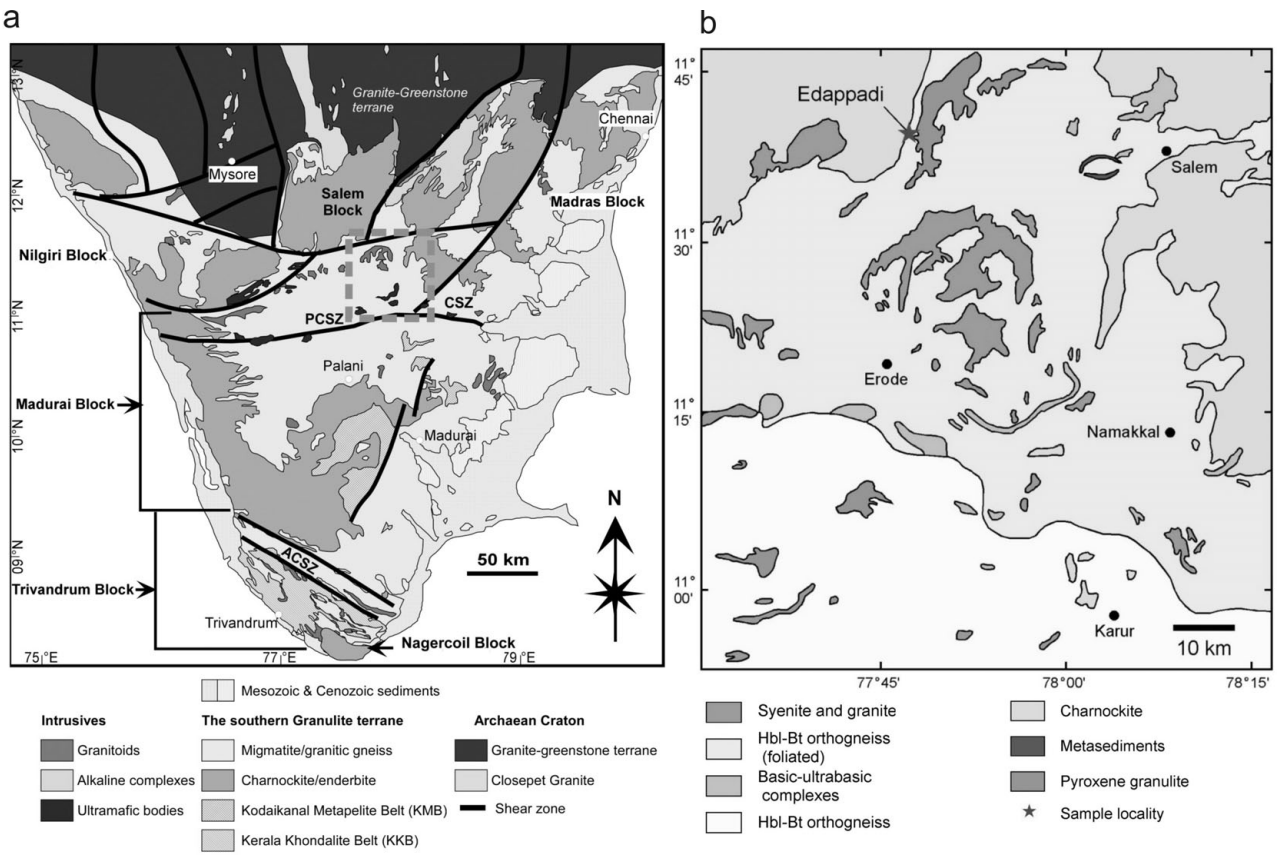

Figure 1. (a) Geological framework of southern India (after Santosh & Sajeev, 2006). The area covered in (b) is shown within box. (b) Geological map of the Palghat-Cauvery Suture Zone area showing the location of present study (based on 1:500 000 map of Tamil Nadu, GSI, 1995). A colour version of this figure is available at http://www.cambridge.org/journals/geo.

the Palghat-Cauvery Suture Zone in southern India (Fig. 1a), a region considered in recent studies as the trace of the Mozambique Ocean closure and subduction–accretion–collision processes associated with the final assembly of the Gondwana supercontinent in the Late Neoproterozoic–Cambrian (Collins *et al.* 2007; Santosh, Maruyama & Yamamoto, 2009; Santosh, Maruyama & Sato, 2009). This is the first report which characterizes the diopsidites within this collisional suture and has important implications for elucidating the tectonics of amalgamation of the Gondwana supercontinent.

2. Geological setting

Southern India occupies a central position in the Late Neoproterozoic–Cambrian Gondwana supercontinent assembly (Santosh, Maruyama & Yamamoto, 2009). The boundary between the Archaean Dharwar Craton in the north and the Neoproterozoic Southern Granulite Terrane in the south is marked by the Palghat-Cauvery Suture Zone (PCSZ) (Chetty *et al.* 2006 and references therein; Collins *et al.* 2007; Clark *et al.* 2009). This zone is considered as the trace of the suture along which the Gondwana supercontinent was finally assembled during Neoproterozoic–Cambrian times. The PCSZ extends westwards into Madagascar as the Betsimisaraka suture that separates the Archaean Antongil craton to the east from the Antananarivo granulite-facies Neoproterozoic orogenic belt to the west (Collins & Windley, 2002), and continues eastwards into Antarctica where it marks the junction between the Napier and Rayner complexes in Enderby Land (Harris, Santosh & Taylor, 1994). Geochronological data including U–Pb zircon and EPMA monazite ages indicate that the rocks along the PCSZ underwent an episode of high-grade metamorphism at *c*. 530 Ma (Collins *et al.* 2007; Santosh *et al.* 2006) that broadly coincides with the time of final assembly of the Gondwana supercontinent. The PCSZ is interpreted to mark the trace of the Mozambique Ocean closure and in a recent tectonic model; Santosh, Maruyama & Sato (2009) proposed a Pacific-type orogeny culminating in a Himalayan style collision to explain the Neoproterozoic evolution of southern India and its final incorporation within the Gondwana assembly. This model envisages an early rifting stage which gave birth to the Mozambique Ocean, followed by the initiation of southward subduction of the oceanic plate beneath a thick tectosphere-bearing Archaean Dharwar Craton. Slices of dunite–pyroxenite–gabbro sequence invaded by mafic dykes and intruded by plagiogranite are exposed at Manamedu along the southern part the PCSZ (Santosh, Maruyama & Sato, 2009). Evidence for the southward subduction and subsequent northward extrusion are preserved in the PCSZ where the orogenic core carries

https://doi.org/10.1017/S0016756810000154 Published online by Cambridge University Press

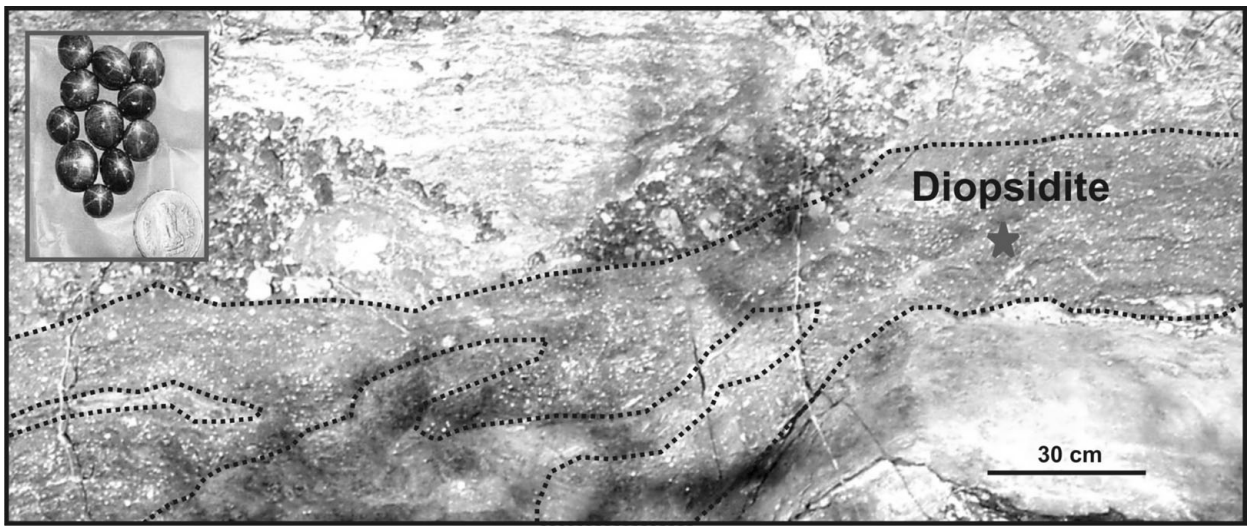

Figure 2. Field photograph of diopsidite dykes occurring as veins and dykes within altered gabbroic rocks. The sample location is shown by star. The inset shows cut and polished diopside crystals from the diopsidites sold as a semi-precious stones in the local gem market. A colour version of this figure is available at http://www.cambridge.org/journals/geo.

high-pressure and ultrahigh-temperature metamorphic assemblages with ages corresponding to the Cambrian collisional orogeny (Shimpo, Tsunogae & Santosh, 2006; Ohyama, Tsunogae & Santosh, 2008; Tsunogae *et al.* 2008). Several high-pressure mafic granulites (metagabbros) and garnet amphibolites representing subduction of oceanic crust were recently reported from the PCSZ (Santosh *et al.* 2010). Numerous occurrences of Mg–Al rich mafic gneisses have been reported in recent studies from several localities within the PCSZ (Santosh, Tsunogae & Koshimoto, 2004; Santosh & Sajeev, 2006; Shimpo, Tsunogae & Santosh, 2006; Collins *et al.* 2007; Tsunogae *et al.* 2008). The *P–T* data show that these rocks experienced high-pressure (HP, pressures up to 15–20 kbar) metamorphism, followed by ultrahigh-temperature (UHT, temperatures up to 1000 °C) conditions in a convergent tectonic regime (Shimpo, Tsunogae & Santosh, 2006; Santosh & Sajeev, 2006; Collins *et al.* 2007; Tsunogae *et al.* 2008). The close association of ultramafic rocks having abyssal signatures together with linear belts of iron formation and metachert in several localities within the PCSZ probably represents a subduction–accretion setting (Santosh, Maruyama & Sato, 2009). Fragments of the mantle wedge were brought up through extrusion tectonics and these fragments now occur as suprasubduction zone/arc assemblages including chromitites, highly depleted dunites, and pyroxene-bearing ultramafic assemblages. Extensive CO_2 metasomatism of the ultramafic units generated magnesite deposits (Santosh, Maruyama & Sato, 2009). The crustal flower structure mapped from PCSZ (Chetty & Bhaskar Rao, 2006) supports an extrusion model, and the large-scale north-verging thrusts towards the north of the orogenic core may represent a fold-thrust belt. Towards the south of the PCSZ is the Madurai Block, where evidence for extensive magmatism occurs, represented by a number of granitic plutons and igneous charnockite massifs of possible tonalite–trondhjemite–granodiorite (TTG) setting, with ages ranging from *c*. 750 to 560 Ma, suggesting a long-lived Neoproterozoic magmatic arc within a > 200 km wide belt (Santosh, Maruyama & Sato, 2009). All these magmatic units were subsequently metamorphosed, when the Pacific-type orogeny switched over to collision-type in Cambrian times, during the final phase of assembly of the Gondwana supercontinent. The occurrence of arc magmatic rocks together with high *P/T* rocks is considered to represent the deeply eroded roots of the arc. The final phase of the orogeny witnessed the closure of the Mozambique Ocean and the collisional assembly of continental fragments within the Gondwana supercontinent amalgam. Thus, Santosh, Maruyama & Sato (2009) proposed that the tectonic history of southern India represents a progressive sequence from Pacific-type to collision-type orogeny which finally gave rise to a Himalayan-type Cambrian orogen with characteristic magmatic, metasomatic and metamorphic factories operating in a subduction–collision setting.

The occurrence of diopsidite dykes in a number of localities within the PCSZ, including Adayur, Edappadi and Poolampatti, was first recorded by Santosh, Maruyama & Sato (2009). In this study, we examined the diopsidite dykes at Edappadi (Fig. 1b) at the northern margin of the PCSZ (location co-ordinates: N11°39.877′, E77°46.725′). Here, concordant as well as discordant dykes and veins of dark and coarse-grained diopside-rich rocks occur within altered gabbroic rocks (Fig. 2). Except for the formation of late hydrous minerals, there is no evidence for any subsequent high-*T* effects, and therefore these dykes are considered to have been emplaced after the high-grade metamorphism, although they were affected by retrograde metamorphic effects. The dykes and veins range in thickness from a few centimetres

https://doi.org/10.1017/S0016756810000154 Published online by Cambridge University Press

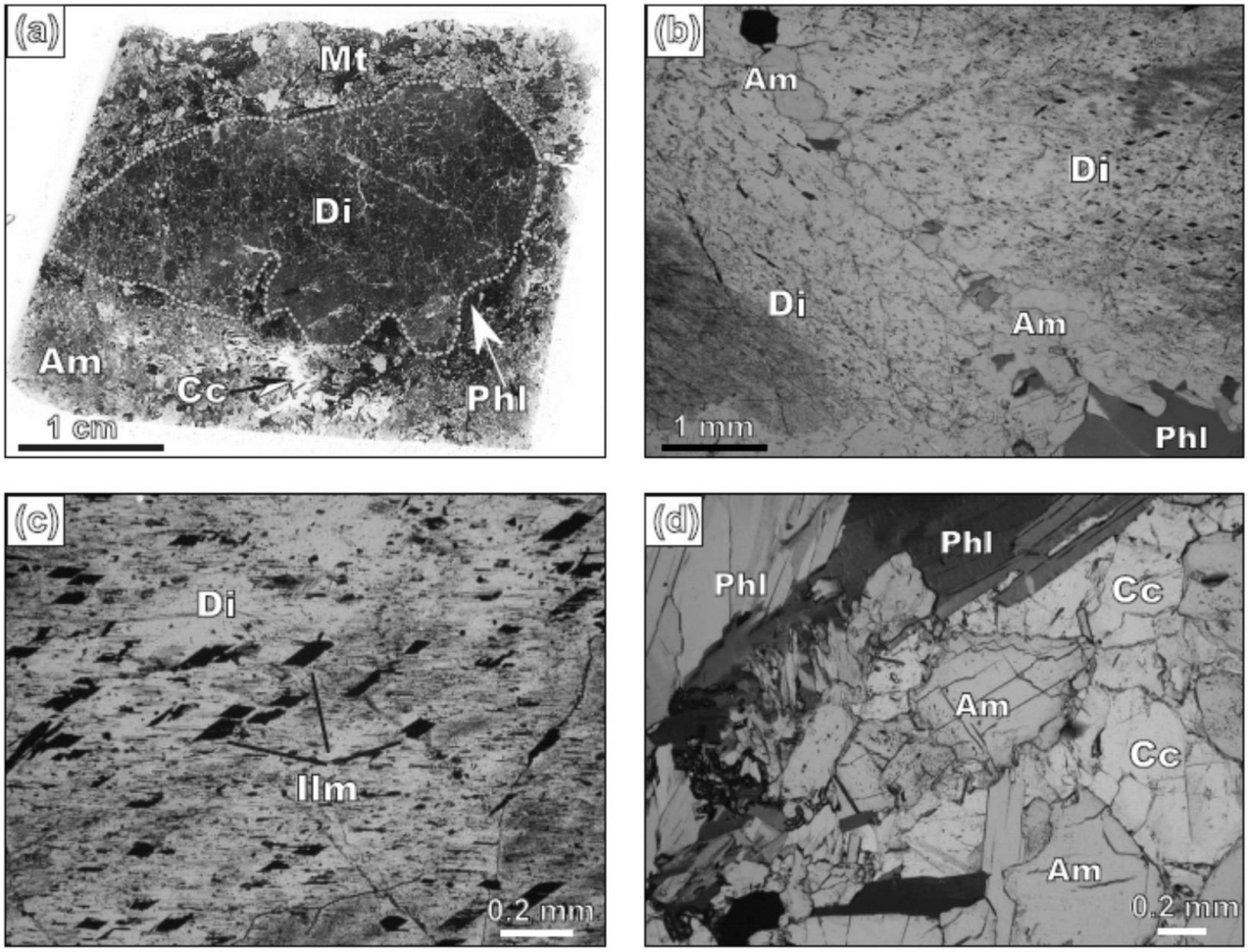

Figure 3. Thin-section photomicrographs showing representative textures of the diopsidite sample. All photos under polarized light except (b) and (d) which are under crossed polars. (a, b) Highly coarse-grained diopside (Di) crystals surrounded by secondary calcic amphiboles (Am), phlogopite (Phl) and magnetite (Mt). (c) Numerous thin lamellae of ilmenite (Ilm) occur in the core of coarse-grained diopside. (d) Calcite (Cc)-bearing portion of the rocks showing calcic amphibole-calcite association. A colour version of this figure is available at http://www.cambridge.org/journals/geo.

up to several tens of centimetres and appear to fill former cracks, similar to those reported from the Oman ophiolites (Python *et al.* 2007*b*). Although the layered gabbros in the Manamedu complex at the southern margin of the PCSZ are associated with other mafic/ultramafic lithologies such as dunite, pyroxenite and hornblendite, in the present locality, such an association is not evident. The formation of hydrous minerals at the contact resembles the common presence of hydrous minerals such as antigorite and tremolite at the contact between host periodotite and diopsidite dykes in the mantle section of Oman ophiolite (Python *et al.* 2007*a*,*b*). The layering in the host gabbros in the present case is considered to be the relict of a primary layering similar to the layered gabbros in various gabbroic complexes, including the Manamedu complex within the PCSZ (Santosh, Maruyama & Sato, 2009).

The diopsidites are locally mined for the large (up to 6 cm) and shiny crystals of diopside which are cut, polished and sold in the gem market with a local trade name of 'black cat's eye' (Fig. 2, inset).

3. Petrography

A large number of thin-sections prepared from several samples of the diopsidite collected from Edappadi were examined. Since no major variation in mineralogy was observed, a representative sample (sample number MD 16–6) was chosen for detailed analytical work in the present study. The general texture of dykes is characterized by coarse diopside crystals (~ 80 %) surrounded by medium-grained hornblende (~ 10 %), phlogopite (~ 6 %) and plagioclase (2–5 %) (Fig. 3). Accessory minerals are titanite, magnetite and calcite. Diopside is very coarse grained (several millimetres or up to few centimetres in length) and subhedral and is commonly surrounded by secondary calcic amphibole (0.4–2.0 mm, up to 4 mm) and phlogopite (0.2–4.5 mm, up to 12 mm) (Fig. 3a, b) along with minor plagioclase (0.2–1.2 mm), suggesting their formation either during late stages of fluid activity after crystallization of the diopside or during retrograde metamorphism under amphibolite-facies conditions. Cr-spinel and olivine were not identified in the diopsidites. The core of

https://doi.org/10.1017/S0016756810000154 Published online by Cambridge University Press

the coarse-grained diopside contains numerous thin lamellae of ilmenite, probably formed by exsolution during cooling after crystallization at high temperatures (Fig. 3c). Some phlogopite, calcite and magnetite are found as inclusions within coarse diopside grains, but they are fracture controlled, indicating their formation after diopside grains. A few small euhedral titanite grains found as inclusions in diopside grains probably indicate their crystallization along with diopsides. Titanite (0.05–1.2 mm) is also present in the aggregate and is associated with phlogopite as a retrograde phase. Calcite is also present with calcic amphibole and phlogopite in the plagioclase-free portions of the rock, forming calcite-rich domains (Fig. 3d). There is no textural evidence for either the replacement of a primary mineral by later clinopyroxene or its occurrence along cracks/fractures/cleavage planes in primary minerals. Instead, the coarse-grained and fresh diopsides are the predominant primary mineral. The occurrence and textural characteristics therefore do not favour a simple model of mantle metasomatism and/or prograde metamorphism for the formation of diopsides.

4. Mineral chemistry

4.a. Analytical methods

Major element analyses of the constituent minerals were carried out using an electron microprobe analyser (JEOL JXA8621) at the Chemical Analysis Division of the Research Facility Center for Science and Technology, the University of Tsukuba. The analyses were performed under conditions of 20 kV accelerating voltage and 10 nA sample current, and the data were regressed using an oxide-ZAF correction program supplied by JEOL.

Trace and rare earth element concentrations in the diopside were determined using a laser ablation (193 nm ArF excimer: MicroLas GeoLas Q-plus)-inductively coupled plasma mass spectrometry (LA-ICP-MS; Agilent 7500S) at the Department of Earth Sciences, Kanazawa University, Japan. Each analysis was carried out by ablating an area of 50 μm diameter spots for diopside at 5 Hz with an energy density of 8 J cm^{-2} per pulse. We used NIST SRM 612 glass as a primary calibration standard, which was analysed routinely at the beginning of a batch of 3–4 diopside spots with a linear drift correction applied between each calibration. We preferred the element concentration values recommended by Pearce *et al.* (1997) for NIST SRM 612 glass for calibration. Data reduction was subsequently performed following a protocol defined by Longerich, Jackson & Gunther (1996), using Si as internal standard based on the values of SiO_2 (in wt %) obtained by EPMA analyses. The analytical details and data quality are the same as those reported in Ishida *et al.* (2004) and Morishita *et al.* (2004).

4.b. Results

Representative major element compositions of minerals from the diopsidite in PCSZ are given in Tables 1 and 2. The trace and rare earth element compositions of the diopside are given in Table 3.

4.b.1. Diopside

The diopside grains show high Mg no. (100 $Mg/(Mg+Fe^{tot})$) with the grain cores possessing higher values (84–89) when compared to their rims (79–83). The cores also have high CaO concentrations. The diopsides show low values of Cr, Al and Ti. The rims of coarse-diopside grains are enriched in Na and Fe. The data plot in the field of diopside within the pyroxene ternary diagram (not shown) with cores having an average composition of $En_{44}Wo_{49}Fs_7$. The Ca/(Ca+Na+K) values are higher for cores (up to 0.98) as compared to the rims (0.88 to 0.92) (Table 1). The diopside grains in this rock are highly coarse-grained and it is common for such grains to preserve chemical zoning. There is marked enrichment in Fe and depletion in Ca from the core to rim. However, the Na_2O content in rims is higher than that of the diopsides described from similar settings as well as oceanic gabbros and basalts. We interpret this elemental zoning to reflect the progressive evolution of the concentration of the various elements in the fluids/melts from which the mineral crystallized, probably combined with later retrograde metamorphism.

On a chondrite-normalized REE diagram (Fig. 5a), with REE normalization following Sun & McDonough (1989), the diopside data show a convex-upward pattern for LREEs, although the $(La/Yb)_N$ values are rather low (0.2–0.5). The LREE abundance is moderately higher than those for clinopyroxenes reported from some of the ultramafic units in ophiolites and/or fore-arc mantle peridotites (e.g. Tamura & Arai, 2006; Kelemen, Shimizu & Salters, 1995; Parkinson *et al.* 1992). A significant Eu anomaly is also not observed in the analysed diopside grains (Eu/Eu^* ranges from 0.8 to 1.0). The data show low values for high field strength elements (HFSEs) like Nb, Ti, Hf and Zr. Ta concentrations are below detection limits. Prominent negative anomalies for Nb, Ti and Zr are observed on a primitive mantle normalized (after Sun & McDonough, 1989) spidergram (Fig. 5b). Pb displays a positive anomaly together with Sr (Fig. 5b), which most likely suggests involvement of subduction components associated with the formation of these rocks (e.g. Dilek, Furnes & Shallo, 2008).

4.b.2. Other minerals

The mica (phlogopite) is Mg-rich and characterized by low-TiO_2 content (Table 2). Inclusions of phlogopite within diopside are slightly Mg-rich (Mg no. = 0.76) as compared to those in the matrix phase (0.71–0.75), although the TiO_2 contents of both the matrix and

https://doi.org/10.1017/S0016756810000154 Published online by Cambridge University Press

Table 1. Representative major element analyses of diopside in diopsidites

Rec. no.	175	176	164	165	166	167	173	174	171	172	
Sample no.	MD16–6 coarse-grain (core)	MD16–6 coarse-grain (core)	MD16–6 core	MD16–6 core	MD16–6 rim	MD16–6 rim	MD16–6 rim	MD16–6 rim	MD16–6 rim	MD16–6 rim	
Analysis no.	12	13	1	2	3	4	10	11	8	9	
SiO_2 (wt %)	53.51	53.22	54.12	53.80	53.56	53.96	54.70	54.19	54.17	53.77	
Al_2O_3	0.60	0.69	0.37	0.44	0.65	0.61	0.51	0.60	0.56	0.49	
TiO_2	0.09	0.04	0.02	0.00	0.05	0.02	0.05	0.02	0.07	0.02	
Cr_2O_3	0.00	0.00	0.00	0.00	0.01	0.00	0.04	0.05	0.00	0.03	
FeO	3.62	3.43	5.21	4.89	6.65	6.59	5.45	6.51	5.83	5.41	
MnO	0.13	0.10	0.09	0.13	0.15	0.13	0.16	0.11	0.15	0.22	
MgO	15.77	15.75	15.16	15.38	13.99	14.32	14.59	14.20	14.63	14.85	
CaO	24.76	24.81	23.77	23.92	22.79	22.59	23.27	22.75	23.47	23.60	
Na_2O	0.35	0.26	0.91	0.79	1.65	1.76	1.13	1.55	1.00	1.03	
K_2O	0.00	0.00	0.02	0.00	0.01	0.01	0.02	0.05	0.01	0.00	
ZnO	0.04	0.00	0.00	0.01	0.03	0.00	0.07	0.02	0.00	0.00	
Total	98.87	98.30	99.67	99.35	99.54	99.99	99.99	100.04	99.87	99.41	
Cations on the basis of 6 oxygen atoms											
Si	1.985	1.984	2.001	1.994	1.997	2.000	2.014	2.005	2.002	1.997	
Al	0.026	0.030	0.016	0.019	0.029	0.027	0.022	0.026	0.024	0.021	
Ti	0.003	0.001	0.000	0.000	0.001	0.001	0.001	0.001	0.002	0.001	
Cr	0.000	0.000	0.000	0.000	0.000	0.000	0.001	0.001	0.000	0.001	
Fe2+	0.112	0.107	0.161	0.152	0.207	0.204	0.168	0.201	0.180	0.168	
Mn	0.004	0.003	0.003	0.004	0.005	0.004	0.005	0.003	0.005	0.007	
Mg	0.871	0.875	0.835	0.849	0.777	0.790	0.801	0.783	0.805	0.822	
Ca	0.984	0.991	0.941	0.950	0.910	0.897	0.918	0.902	0.929	0.938	
Na	0.025	0.019	0.065	0.056	0.119	0.126	0.080	0.111	0.071	0.074	
K	0.000	0.000	0.001	0.000	0.001	0.000	0.001	0.002	0.000	0.000	
Zn	0.001	0.000	0.000	0.000	0.001	0.000	0.002	0.001	0.000	0.000	
Total	4.012	4.009	4.024	4.024	4.047	4.050	4.013	4.037	4.020	4.028	
$Mg/(Mg+Fe^{tot})$	0.89	0.89	0.84	0.85		0.79	0.79	0.83	0.80	0.82	0.83
Ca/(Ca+Na+K)	0.98	0.98	0.93	0.94	0.88	0.88	0.92	0.89	0.93	0.93	
Mg/(Fe+Mg+Ca+Mn)	0.44	0.44	0.43	0.43		0.41	0.42	0.42	0.41	0.42	0.42
Fs	0.06	0.06	0.08	0.07		0.11	0.11	0.09	0.11	0.09	0.09
En	0.44	0.44	0.43	0.44	0.41	0.42	0.42	0.41	0.42	0.42	
Wo	0.50	0.50	0.49	0.49		0.48	0.47	0.49	0.48	0.49	0.49

Table 2. Representative analyses of accessory minerals in diopsidites

Rec. no.	61	63	71	72	70	70
Sample no.	MD16–6	MD16–6	MD16–6	MD16–6	MD16–6	MD16–6
Mineral name	phlogopite	phlogopite	hornblende	hornblende	titanite	plagioclase
O*	22	22	23	23	5	8
Remarks	matrix	in Cpx	core	rim		
SiO_2	39.24	39.25	53.73	53.59	29.92	68.95
Al_2O_3	13.37	13.15	3.31	3.44	0.77	0.01
TiO_2	1.09	1.14	0.15	0.08	37.74	19.50
Cr_2O_3	0.00	0.00	0.05	0.02	0.04	0.00
Fe_2O_3					1.23	
FeO	11.67	10.91	5.57	5.69		0.13
MnO	0.07	0.11	0.09	0.08	0.00	0.01
MgO	19.14	19.03	19.67	19.82	0.00	0.00
CaO	0.01	0.02	12.56	12.58	28.84	0.27
Na_2O	0.14	0.09	1.04	1.07	0.00	11.09
K_2O	9.95	9.91	0.25	0.26	0.00	0.05
ZnO	0.00	0.01	0.00	0.04	0.00	0.00
Total	94.69	93.62	96.41	96.67	98.54	100.01
Si	5.811	5.856	7.617	7.587	0.995	3.005
Al	2.332	2.312	0.553	0.573	0.030	1.001
Ti	0.121	0.128	0.016	0.009	0.944	0.000
Cr	0.000	0.000	0.005	0.002	0.001	0.000
$Fe3^+$					0.031	
Fe^{2+}	1.444	1.361	0.660	0.674		0.000
Mn	0.009	0.014	0.011	0.009	0.000	0.005
Mg	4.222	4.229	4.153	4.180	0.000	0.000
Ca	0.002	0.004	1.906	1.907	1.028	0.013
Na	0.041	0.026	0.287	0.294	0.000	0.936
K	1.879	1.885	0.044	0.046	0.000	0.003
Zn	0.000	0.001	0.000	0.004	0.000	0.000
Total	15.862	15.816	15.253	15.286	3.030	4.963
Mg/(Fe+Mg)	0.75	0.76	0.86	0.86		

*number of oxygens

Table 3. Representative trace and rare earth element analyses of diopside in diopsidites (sample no. MD 16–6)

Analysis no.	201 core	202 core	203 core	204 rim	205 core	206 core	207 rim	208 core
Li (ppm)	12.68	12.91	12.10	12.27	11.55	11.18	9.82	12.35
Ti	160.41	157.46	163.35	141.94	164.71	153.97	130.12	165.01
Rb	0.04	bdl	bdl	bdl	bdl	bdl	bdl	bdl
Sr	104.93	105.77	114.78	83.21	117.35	115.33	83.97	107.11
Y	4.77	4.77	5.23	4.10	5.51	5.21	2.42	4.56
Zr	5.84	6.07	6.28	5.00	6.42	6.14	4.42	6.46
Nb	0.02	0.02	0.02	0.02	0.02	0.03	0.02	0.03
Ba	bdl	0.09	bdl	bdl	bdl	bdl	0.10	0.20
La	0.33	0.33	0.36	0.16	0.41	0.38	0.12	0.28
Ce	2.31	2.31	2.55	1.29	2.86	2.75	0.85	2.10
Pr	0.58	0.57	0.63	0.36	0.71	0.66	0.21	0.54
Nd	3.76	3.59	4.29	2.58	4.64	4.29	1.55	3.49
Sm	1.53	1.46	1.67	1.22	1.84	1.69	0.71	1.45
Eu	0.41	0.41	0.46	0.35	0.48	0.45	0.20	0.44
Gd	1.42	1.38	1.56	1.20	1.65	1.53	0.70	1.32
Tb	0.19	0.20	0.20	0.16	0.21	0.20	0.10	0.18
Dy	1.06	1.06	1.19	0.97	1.24	1.19	0.55	1.01
Ho	0.19	0.18	0.19	0.17	0.21	0.19	0.09	0.18
Er	0.47	0.47	0.51	0.41	0.56	0.51	0.24	0.45
Tm	0.07	0.08	0.07	0.07	0.08	0.08	0.04	0.07
Yb	0.58	0.58	0.59	0.55	0.62	0.60	0.30	0.57
Lu	0.10	0.10	0.10	0.10	0.11	0.10	0.06	0.09
Hf	0.49	0.54	0.49	0.48	0.61	0.56	0.42	0.59
Ta	bdl	bdl	bdl	bdl	bdl	bdl	bdl	bdl
Pb	19.90	19.57	20.48	19.64	20.89	21.06	16.18	27.19
Th	0.01	0.03	bdl	bdl	bdl	0.02	0.07	0.03
U	bdl	0.02	bdl	bdl	bdl	0.02	0.04	0.02
$(La/Yb)_N$	0.4	0.4	0.4	0.2	0.5	0.5	0.3	0.4
Eu/Eu*	0.9	0.9	0.9	0.9	0.8	0.9	0.9	1.0

Note: We used chondrite-normalized (after Sun & McDonough, 1989) for $(La/Yb)_N$ calculations; analyses 201 to 204 correspond to diopside grain no. 3 in Table 1 and 205 to 208 to grain no. 2 in Table 1; bdl – below detection limits

https://doi.org/10.1017/S0016756810000154 Published online by Cambridge University Press

included phases are almost similar (0.6–1.1 wt %). Calcic amphibole, which is classified as actinolite or actinolitic hornblende, is also magnesian (Mg no. = 0.80–0.86). It is compositionally nearly homogeneous, and with no significant compositional difference between the core and rim of grain. The mineral also contains minor Na_2O (1.0–1.8 wt %), K_2O (0.2–0.4 wt %) and TiO_2 (0.1–0.2 wt %). Titanite composition is close to its ideal formula with minor Fe_2O_3 (1.1–1.6 wt %) and Al_2O_3 (0.6–1.9 wt %). Plagioclase associated with phlogopite and calcic amphibole is albite-rich with a composition $An_{1–2}$. Calcite composition is also close to $CaCO_3$ with very minor FeO (0.1–0.5 wt %) and MgO (0–0.5 wt %).

5. Discussion

The possible genetic mechanisms proposed for the formation of diopsidites/clinopyroxenites include: (1) magmatic crystallization, (2) metasomatism and metamorphism, and (3) high- or low-temperature hydrothermal fluid circulation in ultramafic lithologies in the oceanic realm (e.g. Dantas *et al.* 2007; Dilek, Furnes & Shallo, 2008; Ishiwatari *et al.* 2006; Python *et al.* 2007*a*,*b*; Python & Arai, 2009; Grégoire *et al.* 2000; Grégoire, McInnes & O'Reilly, 2001; Bach & Klein, 2009).

5.a. Are diopsidite dykes formed by igneous processes?

Magmatic diopsidite/clinopyroxenite veins/dykes are quite abundant in various igneous settings. They are more common in oceanic environments, particularly occurring as dykes within the mantle and crustal rocks in many ophiolitic terrains. A magmatic origin is generally proposed for those Mg-rich diopsidite dykes which appear as millimetric to centimetric layers parallel to the bedding of layered gabbros, or as intrusions, dykes and bodies in crustal or mantle sections (Ernewein, Pfumio & Whitechurch, 1988; Dantas *et al.* 2007; Dilek, Furnes & Shallo, 2008). Mantle clinopyroxenes usually have Cr_2O_3 in the range of 0.5 to 2.5 wt % and the value in mafic–ultramafic cumulates varies from 0.22 to 1 wt % (Python & Ceuleneer, 2003; Tamura & Arai, 2006; Elthon, Stewart & Ross, 1992; Parlak, Höck & Delaloye, 2000). The Al_2O_3 contents in clinopyroxenes in mantle peridotites and ultramafic–mafic cumulate or non-cumulate rocks are usually higher than 1 wt %. The Mg numbers of the coarse diopside grains in the PCSZ range as high as 89, which is within the range of magmatic values. However, these diopside grains have much lower values for Al, Ti and Cr, and high contents of Na (towards the rim), when compared to magmatic clinopyroxenes from various rocks (Python *et al.* 2007*a*,*b*; Tamura & Arai, 2006; Zhang, Ying & Shimoda, 2007). The data (core compositions) plot away from igneous field on diagrams such as Al_2O_3 v. Mg no. and Na_2O v. Mg no. (Fig. 4a, b). The Cr_2O_3 contents of clinopyroxene are dependent on Mg no., that is, as Mg no. increases,

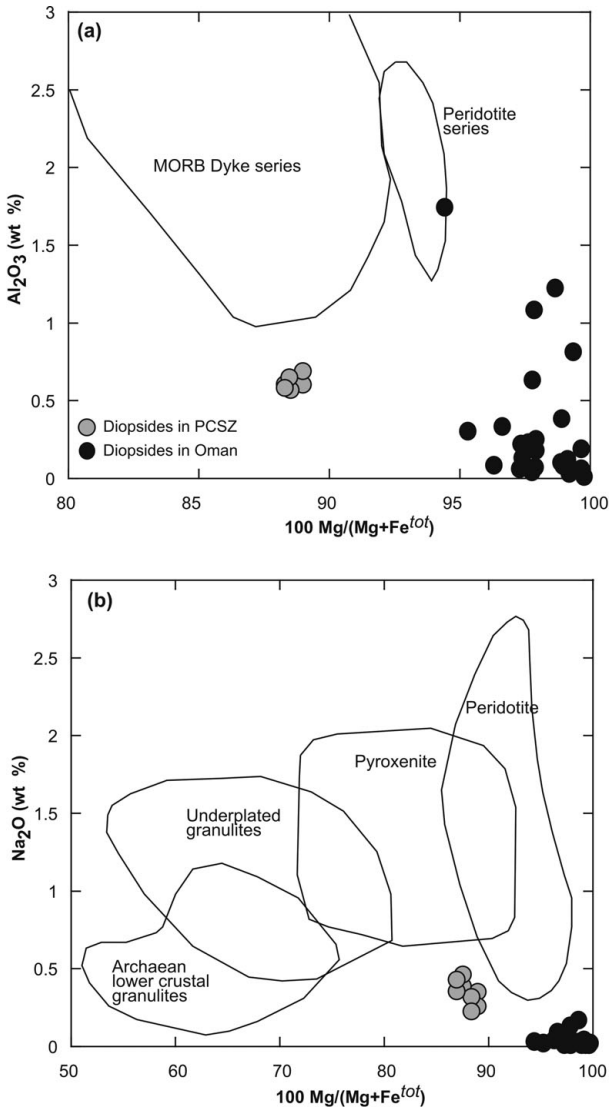

Figure 4. (a) Mg no. v. Al_2O_3 (wt %) diagram (cf. Python *et al.* 2007*a*,*b*) and (b) Mg no. v. Na_2O (wt %) diagram (after Zhang, Ying & Shimoda, 2007). Only the most Mg-rich core compositions have been used in diagrams (a) and (b).

Cr_2O_3 will also increase and vice versa, a process that is related to the depletion of these elements in magma/melts (Hodges & Papike, 1976; Parlak, Höck & Delaloye, 2000, 2002) during differentiation. Olivine and Cr-spinels are not observed in the studied sections and no olivine + Cr-spinel-rich rocks were identified in the study area. Hence, we infer that the diopsidites from PCSZ may not be related to an earlier fractionation of olivine and spinel from melts/fluids which would have caused a depletion of Mg and Cr in the more evolved melts. Cr content in other minerals such as amphibole, phlogopite and magnetite is very low; hence, we discard the possibility of retention of Cr in other phases of the rock. The absence of cogenetic ilmenite, K-richterite and rutile along with calcic pyroxene in the rock precludes the possibility of involvement of silicate melts in the genesis of the diopsidites (e.g. Harte, Hunter & Kinny, 1993). The major element mineral

https://doi.org/10.1017/S0016756810000154 Published online by Cambridge University Press

chemical characteristics combined with textural features of the diopsidites do not favour their genesis through magmatic processes such as fractional crystallization and/or crystal accumulation in a magmatic chamber.

5.b. Are diopsidite dykes formed by metasomatic/metamorphic processes?

Clinopyroxenites usually occur as veins in cratonic mantle peridotites and provide vital textural evidence for mantle metasomatism. These metasomatic clinopyroxenes are characterized by strong enrichment in LREEs and incompatible elements (e.g. Kempton *et al.* 1999; Van Achterbergh, Griffin & Stiefenhofer, 2001), together with strong enrichment in Na_2O and Cr_2O_3 (Grégoire *et al.* 2000), depending on the nature of the metasomatic agent. Nozaka (2005) reported retrograde clinopyroxenes with low Al, Na, Ti and Cr with high Mg no. (96) in Happo-O'ne metaperidotite. Their clinopyroxenes show clear textural evidence for retrograde formation. The diopside from the Palghat-Cauvery Suture Zone is a predominantly primary mineral that underwent subsequent retrograde metamorphism generating minor hydrous minerals. The occurrence as dykes, and lack of significant textural evidence for metasomatic/metamorphic reactions, combined with chemical characteristics, do not favour a metasomatic/metamorphic origin for diopsidites in the PCSZ. Also, typical minerals associated with metamorphic calc-silicate rocks such as scapolite, wollastonite and calcic plagioclase are absent in the present case.

5.c. Role of subduction-derived fluids in the formation of diopsidites

We now evaluate the role of fluids in the genesis of these diopsidites. The occurrence of very coarse diopside in this rock suggests the involvement of H_2O and Ca-rich fluids/melts (e.g. McCollom & Shock, 1998; Python *et al.* 2007*a*,*b*; Sablukova & Sablukov, 2008). The Mg no. of the diopside is less than 90, suggesting their crystallization from a fertile source. The diopsides are rich in Sr and LREEs, and depleted in Ti, Nb, Ta and Zr. These features suggest hydrous formation conditions where the LREEs and Sr are incorporated in hydrous fluids such as seawater (Tatsumi, Hamilton & Nesbitt, 1986; Maury, Defant & Joron, 1992; Kogiso, Tatsumi & Nakano, 1997) in a subduction regime. The early crystallization of mica, amphibole and titanite particularly rich in HFSEs might reduce their concentrations in the residual melt. The mica, amphibole and titanite in our diopsidite samples are evidently of later origin related to retrograde metamorphism and Barrovian hydration. These secondary minerals mostly occur along grain boundaries as well as microfractures within the diopside grains. These suggest that the HFSEs do not reside in the above-mentioned phases and their behaviour can be utilized to interpret the source characteristics, particularly the role of fluids. The low Al_2O_3 contents in the diopsides of the present study, correlating with low Cr_2O_3 values, do not support a simple model of crustal contamination for the genesis of these diopsidites. Further, prominent negative Nb anomalies and distinct positive Pb anomalies are indicative of the influence of subduction zone fluids in the source (e.g. Dorais & Tubrett, 2008). A combination of these features leads us to propose that the diopsidites from the PCSZ might have generated from hydrous Ca, Na, Si, and LILE-enriched fluids in a subduction regime.

Python *et al.* (2007*a*,*b*) and Python & Arai (2009) reported diopsidite dykes in Oman ophiolite intruded into depleted harzburgites and interpreted them as a product of high-temperature hydrothermal fluid circulation within the uppermost mantle sections in the ophiolite. The mineral assemblage of these dykes is dominated by diopside (Mg no. = 95–100) with minor anorthite, forsterite, titanite, amphiboles, Cr-rich spinel and calcite. The PCSZ diopsides are characterized by low Cr, Ti and Al, similar to those of the Oman diopsidites. Our data fall within the range of Al_2O_3 contents and have slightly higher Na_2O contents when compared to those in Oman diopsidites (Fig. 4a, b). This suggests the slight Na-rich nature of the fluids involved in the PCSZ. The trace and rare earth element behaviours of diopsides in the PCSZ on primitive and chondrite normalized diagrams (cf. Fig. 5) are also comparable, except for the enrichment factors. The fluids responsible for formation of diopsidites in Oman ophiolites were intruded into more depleted host rocks such as dunite and harzburgite. In contrast, the subduction-derived LILE-enriched hydrous Ca-bearing fluids in the PCSZ invaded gabbroic rocks in generating the diopsides with lower Mg no. and enriched trace and rare earth element patterns, as gabbroic rocks are more evolved in terms of Mg no. and are obviously more enriched than harzburgites. The presence of calcite in thin-sections, and the calcite veinlets filling microcracks as observed in hand specimens, also support the involvement of hydrothermal fluids. Higher amphibole and phlogopite abundance is noticed towards the contact of the dykes with the host rocks, and the central part of dykes is more or less anhydrous. Arai *et al.* (2008), in a recent study on Yugu peridotite in South Korea, demonstrated that shearing/suturing and water supply linked with cooling led to the production of anhydrous high-temperature pyroxene porphyroclasts and lower temperature neoclasts of hydrated amphiboles. The basic processes associated with the formation of diopsidites from PCSZ are similar to those discussed above; particularly the trace and rare earth elements features are comparable with those of diopsidite dykes in Oman ophiolites. Our data suggest that the hydrous, LILE-enriched and HFSE-depleted subduction-derived fluids were instrumental in generating these rocks, and their petrogenesis is linked to the subduction and closure of the Neoproterozoic Mozambique Ocean during the

https://doi.org/10.1017/S0016756810000154 Published online by Cambridge University Press

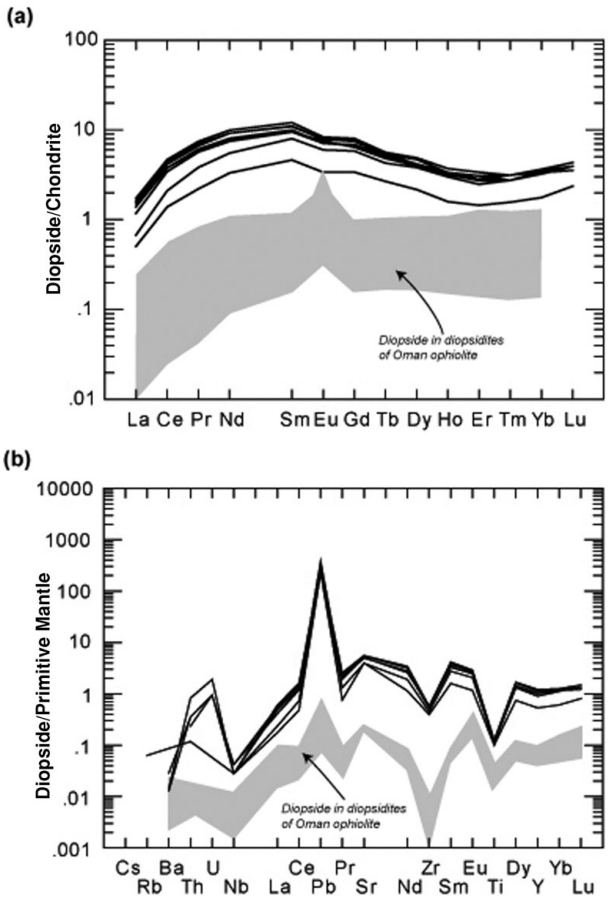

Figure 5. (a, b) Chondrite- and primitive mantle- normalized (after Sun & Mc Donough, 1989) trace and REE patterns for diopsides from the diopsidite rocks in southern India. The shaded area represents data on diopside in diopsidites of Oman ophiolite (from Python *et al.* 2007*a*, *b*).

final assembly of the Gondwana supercontinent in Cambrian times.

Acknowledgements. We thank Dr A. Tamura of Kanazawa University for his valuable help in LA-ICPMS analyses. Drs A. Tamura and S. Ishimaru are thanked for constructive discussions. Comments from two anonymous referees and Dr Marie Python, and editorial suggestions from Prof. David Pyle are highly appreciated. V. J. Rajesh acknowledges the grant-in-aid (P 07331) from the Japan Society for the Promotion of Science (JSPS).

References

ARAI, S., TAMURA, A., ISHIMARU, S., KADOSHIMA, K., LEE, Y.-L. & HISADA, K.-I. 2008. Petrology of the Yugu peridotites in the Gyeonggi Massif, South Korea: Implications for its origin and hydration process. *Island Arc* **17**, 485–501.

BACH, W. & KLEIN, F. 2008. Tales and facts about rodingite and diopsidite in oceanic mantle sections. *Geochimica et Cosmochimica Acta* **72**, A41.

BACH, W. & KLEIN, F. 2009. The petrology of seafloor rodingites: Insights from geochemical reaction path modeling. *Lithos* **112**, 103–17.

CHETTY, T. R. K. & BHASKAR RAO, Y. J. 2006. The Cauvery Shear Zone, Southern Granulite Terrain, India: A crustal-scale flower structure. *Gondwana Research* **10**, 77–85.

CHETTY, T. R. K., FITZSIMONS, I., BROWN, L., DIMRI, V. P. & SANTOSH, M. 2006. Crustal structure and tectonic evolution of Southern Granulite Terrain, India: Introduction. *Gondwana Research* **10**, 3–5.

CLARK, C., COLLINS, A. S., TIMMS, N. E., KINNY, P. D., CHETTY, T. R. K. & SANTOSH, M. 2009. SHRIMP U–Pb age constraints on magmatism and high-grade metamorphism in the Salem Block, southern India. *Gondwana Research* **16**, 27–36.

COLLINS, A. S., CLARK, C., SAJEEV, K., SANTOSH, M., KELSEY, D. E. & HAND, M. 2007. Passage through India: The Mozambique ocean suture, high-pressure granulites and the Palghat-Cauvery Shear System. *Terra Nova* **19**, 141–7.

COLLINS, A. S. & WINDLEY, B. F. 2002. The tectonic evolution of central and northern Madagascar and its place in the final assembly of Gondwana. *Journal of Geology* **110**, 325–40.

DANTAS, C., CEULENEER, G., GRÉGOIRE, M., PYTHON, M., FREYDIER, R., WARREN, J. & DICK, H. J. B. 2007. Pyroxenites from the Southwest Indian Ridge, 9–16°E: Cumulates from Incremental Melt Fractions Produced at the Top of a Cold Melting Regime. *Journal of Petrology* **48**, 647–60.

DILEK, Y., FURNES, H. & SHALLO, M. 2008. Geochemistry of the Jurassic Mirdita Ophiolite (Albania) and the MORB to SSZ evolution of a marginal basin oceanic crust. *Lithos* **100**, 174–209.

DORAIS, M. J. & TUBRETT, M. 2008. Identification of a subduction zone component in the Higganum dike, Central Atlantic Magmatic Province: A LA-ICPMS study of clinopyroxene with implications for flood basalt petrogenesis. *Geochemistry Geophysics Geosystems* **9**, Q10005, doi:10.1029/2008GC002079.

ELTHON, D., STEWART, M. & ROSS, D. K. 1992. Compositional trends of minerals in oceanic cumulates. *Journal of Geophysical Research* **97**, 15189–99.

ERNEWEIN, M., PFUMIO, C. & WHITECHURCH, H. 1988. The death of an accretion zone as evidenced by the magmatic history of the Sumail ophiolite (Oman). *Tectonophysics* **151**, 247–74.

FROST, B. R. 1975. Contact metamorphism of serpentinite, chloritic blackwall and rodingite at Paddy-Go-Easy Pass, Central Cascades, Washington. *Journal of Petrology* **16**, 272–313.

GAGGERO, L., SPADEA, P., CORTESGNO, L., SAVELIEVA, G. N. & PERTSEV, A. N. 1997. Geochemical investigation of the igneous rocks from the Nurali ophiolite mélange zone, southern Urals. *Tectonophysics* **276**, 139–61.

GRÉGOIRE, M., MCINNES, B. I. A. & O'REILLY, S. Y. 2001. Hydrous metasomatism of oceanic sub-arc mantle, Lihir, Papua New Guinea. Part 2: Trace element characteristics of slab-derived fluids. *Lithos* **59**, 91–108.

GRÉGOIRE, M., MOINE, B. N., O'REILLY, S. Y., COTTIN, J. Y. & GIRET, A. 2000. Trace element residence and partitioning in mantle xenoliths metasomatized by highly alkaline, silicate- and carbonate-rich melts (Kerguelen Islands, Indian Ocean). *Journal of Petrology* **41**, 477–509.

GSI (GEOLOGICAL SURVEY OF INDIA). 1995. *Geological and mineral map of Tamil Nadu and Pondicherry*. Geological Survey of India, Calcutta.

HARRIS, N. B. W., SANTOSH, M. & TAYLOR, P. N. 1994. Crustal evolution in South India: constraints from Nd isotopes. *Journal of Geology* **102**, 139–50.

HARTE, B., HUNTER, R. H. & KINNY, P. D. 1993. Melt geometry, movement and crystallization, in relation to mantle dykes, veins and metasomatism. *Philosophical Transactions of the Royal Society of London* **A342**, 1–21.

HODGES, F. N. & PAPIKE, J. J. 1976. DSDP site 334: magmatic cumulates from oceanic layer 3. *Journal of Geophysical Research* **81**, 4135–51.

ISHIDA, Y., MORISHITA, T., ARAI, S. & SHIRASAKA, M. 2004. Simultaneous in-situ multi-element analysis of minerals on thin section using LA–ICP–MS. *The Science Reports of Kanazawa University* **48**, 31–42.

ISHIWATARI, A., YANAGIDA, Y., LI, Y.-B., ISHII, T., HARAGUCHI, S., KOIZUMI, K., ICHIYAMA, Y. & UMEKA, M. 2006. Dredge petrology of the boninite- and adakite-bearing Hahajima Seamount of the Ogasawara (Bonin) forearc: An ophiolite or a serpentinite seamount? *Island Arc* **15**, 102–18.

JAN, Q. M. & HOWIE, R. A. 1981. The mineralogy and geochemistry of the metamorphosed basic and ultrabasic rocks of the Jijal Complex, Kohistan, NW Pakistan. *Journal of Petrology* **22**, 85–126.

KELEMEN, P. B., SHIMIZU, N. & SALTERS, V. J. M. 1995. Extraction of midocean-ridge basalt from the upwelling mantle by focused flow of melt in dunite channels. *Nature* **375**, 747–53.

KEMPTON, P. D., HAWKESWORTH, C. J., LOPEZ-ESCOBAR, L., PEARSON, D. G. & WARE, A. J. 1999. Spinel ± garnet lherzolite xenoliths from Pali Aike, Part 2: trace element and isotopic evidence on the evolution of lithospheric mantle beneath southern Patagonia. In *The J. B. Dawson Volume, Proceedings of the 7th International Kimberlite Conference* (eds J. J. Gurney, J. L. Gurney, M. D. Pascoe & S. H. Richardson), pp. 415–18. Cape Town: Red Roof Design.

KOGISO, T., TATSUMI, Y. & NAKANO, S. 1997. Trace element transport during dehydration processes in the subducted oceanic crust: 1. Experiments and implications for the origin of oceanic island basalts. *Earth and Planetary Science Letters* **148**, 193–206.

LONGERICH, H. P., JACKSON, S. E. & GUNTHER, D. 1996. Laser ablation inductively coupled plasma mass spectrometric transient signal data acquisition and analyte concentration calculation. *Journal of Analytical Atomic Spectrometry* **11**, 899–904.

MAURY, R. C., DEFANT, M. J. & JORON, J.-C. 1992. Metasomatism of the sub-arc mantle inferred from trace elements in Philippine xenoliths. *Nature* **360**, 661–3.

MCCOLLOM, T. M. & SHOCK, E. L. 1998. Fluid–rock interactions in the lower oceanic crust: thermodynamic models of hydrothermal alteration. *Journal of Geophysical Research* **103**, 547–75.

MORISHITA, T., ISHIDA, Y., ARAI, S. & SHIRASAKA, M. 2004. Determination of multiple trace element compositions in thin (30 μm) layers of NIST SRM 614 and 616 using laser ablation–inductively coupled plasma–mass spectrometry. *Geostandards and Geoanalytical Research* **29**, 107–22.

NOZAKA, T. 2005. Metamorphic history of serpentinite mylonites from the Happo ultramafic complex, central Japan. *Journal of Metamorphic Geology* **23**, 711–23.

OHYAMA, H., TSUNOGAE, T. & SANTOSH, M. 2008. CO_2-rich fluid inclusions in staurolite and associated minerals in a high-pressure ultrahigh-temperature granulite from the Gondwana suture in southern India. *Lithos* **101**, 177–90.

PARKINSON, I. J., PEARCE, J. A., THIRLWALL, M. F., JOHNSON, K. T. M. & INGRAM, G. 1992. Trace element geochemistry of peridotites from the Izu–Bonin–Mariana forearc. In *Proceedings of the Ocean Drilling Program, Scientific Results, vol. 125* (eds P. Fryer, J. A. Pearce & L. B. Stokking), pp. 487–506. College Station, Texas.

PARLAK, O., HÖCK, V. & DELALOYE, M. 2000. Suprasubduction zone origin of the Pozantı–Karsantı ophiolite (southern Turkey) deduced from whole-rock and mineral chemistry of the gabbroic cumulates. In *Tectonics and Magmatism in Turkey and the Surrounding Area* (eds E. Bozkurt, J. A. Winchester & J. D. A. Piper), pp. 219–34. Geological Society of London, Special Publication no. 173.

PARLAK, O., HÖCK, V. & DELALOYE, M. 2002. The suprasubduction zone Pozanti–Karsanti ophiolite, southern Turkey: evidence for high-pressure crystal fractionation of ultramafic cumulates. *Lithos* **65**, 205–24.

PEARCE, N. J. G., PERKINS, W. T., WESTGATE, J. A., GORTON, M. P., JACKSON, S. E., NEAL, C. R. & CHENERY, S. P. 1997. A compilation of new and published major and trace element data for NIST SRM 610 and NIST SRM 612 glass reference materials. *Geostandards Newsletter* **21**, 115–44.

PEDROSA-SOARES, A. C., VIDAL, P., LEONARDOS, O. H. & NEVES, B. B. N. 1998. Neoproterozoic oceanic remnants in eastern Brazil: Further evidence and refutation of an exclusively ensialic evolution for the Araçuaí–West Congo orogen. *Geology* **26**, 519–22.

PYTHON, M. & ARAI, S. 2009. Interactions between high-T hydrothermal fluids and mantle lithologies: evidence from the Oman fossilised spreading centre. *Geophysical Research Abstracts* **11**, EGU2009–12245.

PYTHON, M. & CEULENEER, G. 2003. Nature and distribution of dykes and related melt migration structures in the mantle section of the Oman ophiolite. *Geochemistry Geophysics Geosystems* **4**(7), 8612.

PYTHON, M., CEULENEER, G., ISHIDA, Y. & ARAI, S. 2007*a*. Trace element heterogeneity in hydrothermal diopside: evidence for Ti depletion and Sr-Eu-LREE enrichment during hydrothermal metamorphism of mantle harzburgite. *Journal of Mineralogical and Petrological Sciences* **102**, 143–9.

PYTHON, M., CEULENEER, G., ISHIDA, Y., BARRAT, J.-A. & ARAI, S. 2007*b*. Oman diopsidites: a new lithology diagnostic of very high temperature hydrothermal circulation in mantle peridotite below oceanic spreading centres. *Earth and Planetary Science Letters* **255**, 289–309.

QUANRU, G., GUITANG, P., ZHENG, L., CHEN, Z., FISHER, R. D., SUN, Z., OU, C., DONG, H., WANG, X., LI, S., LOU, X. & FU, H. 2006. The Eastern Himalayan syntaxis: major tectonic domains, ophiolitic mélanges and geologic evolution. *Journal of Asian Earth Sciences* **27**, 265–85.

RICE, J. M. 1983. Metamorphism of rodingites: Part I. Phase relations in a portion of the system CaO–MgO–Al_2O_3–SiO_2–CO_2–H_2O. *American Journal of Science* **283A**, 121–50.

SABLUKOVA, L. I. & SABLUKOV, S. M. 2008. Clinopyroxene–phlogopite rock xenoliths: geochemistry, isotope, age, origin and relationship to Grib pipe kimberlites (Arkhangelsk province). *9th International Kimberlite Conference Extended Abstract* 9IKC-A-00165.

SANTOSH, M., COLLINS, A. S., TAMASHIRO, I., KOSHIMOTO, S., TSUTSUMI, Y. & YOKOYAMA, K. 2006. The timing of ultrahigh-temperature metamorphism in Southern India: U–Th–Pb electron microprobe ages from zircon and monazite in sapphirine-bearing granulites. *Gondwana Research* **10**, 128–55.

SANTOSH, M., MARUYAMA, S. & YAMAMOTO, S. 2009. The making and breaking of supercontinents: Some speculations based on superplumes, superdownwelling and the role of tectosphere. *Gondwana Research* **15**, 324–41.

SANTOSH, M., MARUYAMA, S. & SATO, K. 2009. Anatomy of a Cambrian suture in Gondwana: Pacific-type orogeny in southern India? *Gondwana Research* **16**, 321–41.

SANTOSH, M., TSUNOGAE, T., SHIMIZU, H. & DUBESSY, J. 2010. Fluid characteristics of retrogressed eclogites and mafic granulites from the Cambrian Gondwana suture zone in southern India. *Contributions to Mineralogy and Petrology* **159**, 349–69.

SANTOSH, M. & SAJEEV, K. 2006. Anticlockwise evolution of ultrahigh-temperature granulites within continental collision zone in southern India. *Lithos* **92**, 447–64.

SANTOSH, M., TSUNOGAE, T. & KOSHIMOTO, S. 2004. First report of sapphirine-bearing rocks from the Palghat-Cauvery Shear Zone System, Southern India. *Gondwana Research* **7**, 620–6.

SHIMPO, M., TSUNOGAE, T. & SANTOSH, M. 2006. First report of garnet-corundum rocks from Southern India: implications for prograde high-pressure (eclogite-facies?) metamorphism. *Earth and Planetary Science Letters* **242**, 111–29.

SUN, S.-S. & MCDONOUGH, W. F. 1989. Chemical and isotopic systematics of oceanic basalts: implications for mantle composition and processes. In *Magmatism in the Ocean Basins* (eds A. D. Saunders & M. J. Norry), pp. 313–45. Geological Society of London, Special Publication no. 42.

TAMURA, A. & ARAI, S. 2006. Harzburgite–dunite–orthopyroxenite suite as a record of supra-subduction zone setting for the Oman ophiolite mantle. *Lithos* **90**, 43–56.

TATSUMI, Y., HAMILTON, D. L. & NESBITT, R. W. 1986. Chemical characteristics of fluid phase released from a subducted lithosphere and origin of arc magmas: evidence from high-pressure experiments and natural rocks. *Journal of Volcanology and Geothermal Research* **29**, 293–303.

TSUNOGAE, T., SANTOSH, M., OHYAMA, H. & SATO, K. 2008. High-pressure and ultrahigh-temperature metamorphism at Komateri, northern Madurai Block, southern India. *Journal of Asian Earth Sciences* **33**, 395–413.

VAN ACHTERBERGH, E., GRIFFIN, W. L. & STIEFENHOFER, J. 2001. Metasomatism in mantle xenoliths from the Letlhakane kimberlites: estimation of element fluxes. *Contributions to Mineralogy and Petrology* **141**, 397–414.

YANG, J. J. 2006. Ca-rich garnet–clinopyroxene rocks at Hujialin in the Su-Lu terrane (Eastern China): Deeply subducted arc cumulates? *Journal of Petrology* **47**, 965–90.

ZHANG, H. F., YING, J. F. & SHIMODA, G. 2007. Importance of melt circulation and crust–mantle interaction in the lithospheric evolution beneath the North China Craton: evidence from Mesozoic basalt-borne clinopyroxene xenocrysts and pyroxenite xenoliths. *Lithos* **96**, 67–89.